SANDIA REPORT

SAND2004-5465
Unlimited Release
Printed November 2004

Microsystem Strategies for Sample Preparation in Biological Detection

Conrad D. James, Paul C. Galambos, Murat Okandan, Susan Brozik, Monica Manginell, Andreas Acrivos, Dawn J. Bennett, Boris Khusid

Approved for public release; further dissemination unlimited.

Sandia National Laboratories

Microsystem Strategies for Sample Preparation in Biological Detection

Conrad D. James, Paul C. Galambos
MEMS Device Technologies

Murat Okandan
MEMS Technology S&T

Susan Brozik, Monica Manginell
Microsensors S&T

Andreas Acrivos
The City College of New York
Department of Chemical Engineering

Dawn J. Bennett
University of Maryland Baltimore County
Department of Mechanical Engineering

Boris Khusid
New Jersey Institute of Technology
Department of Mechanical Engineering

Sandia National Laboratories
P.O. Box 5800
Albuquerque, New Mexico 87185-1080

Abstract

This report contains the summary of the "Microfluidic cellular Sample Pretreatment" LDRD project 38622.

The objective of this LDRD was to develop microdevice strategies for dealing with samples to be examined in biological detection systems. This includes three sub-components: namely, microdevice fabrication, sample delivery to the microdevice, and sample processing within the microdevice. The first component of this work focused on utilizing Sandia's surface micromachining technology to fabricate small volume (nanoliter) fluidic systems for processing small quantities of biological samples. The next component was to develop interfaces for the surface-micromachined silicon devices. We partnered with Micronics, a commercial company, to produce fluidic manifolds for sample delivery to our silicon devices. Pressure testing was completed to examine the strength of the bond between the pressure-sensitive adhesive layer and the silicon chip. We are also pursuing several other methods, both in house and external, to develop polymer-based fluidic manifolds for packaging silicon-based microfluidic devices. The second component, sample processing, is divided into two sub-tasks: cell collection and cell lysis. Cell collection was achieved using dielectrophoresis, which employs AC fields to collect cells at energized microelectrodes, while rejecting non-cellular particles. Both live and dead Staph. aureus bacteria have been collected using RF frequency dielectrophoresis. Bacteria have been separated from polystyrene microspheres using frequency-shifting dielectrophoresis. Computational modeling was performed to optimize device separation performance, and to predict particle response to the dielectrophoretic traps. Cell lysis is continuing to be pursued using microactuators to mechanically disrupt cell membranes. Novel thermal actuators, which can generate larger forces than previously tested electrostatic actuators, have been incorporated with and tested with cell lysis devices. Significant cell membrane distortion has been observed, but more experiments need to be conducted to determine the effects of the observed distortion on membrane integrity and cell viability. Finally, we are using a commercial PCR DNA amplification system to determine the limits of detectable sample size, and to examine the amplification of DNA bound to microspheres. Our objective is to use microspheres as capture-and-carry chaperones for small molecules such as DNA and proteins, enabling the capture and concentration of the small molecules using dielectrophoresis. Current tests demonstrated amplification of DNA bound to micron-sized polystyrene microspheres using 20-50 microliter volume size reactions.

Acknowledgements

This Page Intentionally Left Blank

Contents

Figures

Tables

Nomenclature

AC	alternating current
DEP	dielectrophoresis
DNA	deoxyribonucleic acid
pDEP	positive dielectrophoresis
PEEK	poly-ethyl ethylene ketone
RF	radio frequency
nDEP	negative dielectrophoresis
NASA	National Aeronautics and Space Administration
SNL	Sandia National Laboratories
SwIFT^{TM}	Surface Micromachining with Integrated Fluidic Technology

Introduction

A growing threat to US security is the production of biological agents for use against the military and civilian populations. To counter this threat, new tools are needed to unravel cellular mechanisms in order to develop fast biological sensors and to design countermeasure vaccines. High throughput genomic and proteomic technologies and advanced sensors are being used to address the threat. However, dramatic improvements to these technologies are needed, especially in the areas of biological sample collection and preparation.

The problem with current microarray techniques is the volume of sample needed. Current protocols for the extraction of nucleic acid material require sampling from large quantities of cells or tissue. In addition, poor sample preparation (RNA degradation, inferior labeling of the sample, etc.) leads to erroneous conclusions. Protocols for nucleic acid isolation can take up to two days and for the most part the sampling preparation is done manually, introducing errors and inconsistency during each step of the procedure.

We propose to apply a microsystem approach to nucleic acid sample collection and preparation for microarray (genomic-based or sensor-based arrays) analysis. Sandia is in a position to play a unique role in developing the tools needed for small sample analysis. With our expertise in microtechnologies, specifically MEMS and Microsensors, we propose to develop components for integration into an automated microsystem that will allow single cell analysis. An automated microsystem will eliminate any sample-to-sample process variability. In addition, the smaller volumes that one needs for an on-chip microfluidic system (on the order of picoliters to nanoliters) can potentially be processed more cheaply and efficiently than the larger volumes now typically used.

We have refined our original objective of developing a rapid and sensitive cellular identification microsystem. This refinement has led us to broaden the scope of the project, in the sense of truly seeking to produce a microsystem that can detect any biological agent. The primary difficulty with developing such a system is the wide range of analytes that need to be handled and detected. Biological agents come in the form of bacterial cells, fungi, viruses, and toxin molecules. A micro total analytical system for bio-detection needs to be capable of handing analytes from micron-sized cells to nanometer-sized molecules. In addition, the system should be able to detect multiple agents within a single sample. Our strategy is to use microspheres as the bridge between nanometer-sized particles (DNA, toxins, antigens, etc.) and the micro/meso-scale fluidic systems that we have currently developed. We will use the microspheres as capture-and-carry tools for small molecule detection assays. This technology will then be coupled with cell collection methods and cell-lysing microdevices to provide a system capable of identifying biological agents of numerous forms.

We have made significant progress in developing microsystem solutions to sample handling for biological detection systems. Specifically, we developed modular components using surface micromachined silicon devices to provide different functionality in the biological detection sequence of tasks. One assumption is that the sample will be collected using an air sampler, or a drawn sample of fluid (blood, stream water, etc.) – in both cases, the sample will be liquid based, and ready for transport to the

detection system. The first step after acquiring the liquid sample is to collect relevant analytes (cells, viruses, proteins) and remove contaminants (dust, soot, etc.). We have developed a high frequency (~MHz) AC field technique for collecting cellular particles and removing non-cellular particles. This is the first silicon-based device component developed in this LDRD. We have also used modeling to optimize device function by examining the electric field distributions within proposed microdevices.

After the analytes of interest are collected, cells need to lysed in order to access their genetic material for identification. We have developed surface micromachined silicon devices that use mechanical shear in order to lyse cells. We have tested an array of actuators and piston designs in order to facilitate the greatest shear on cell walls and membranes. This was the most difficult task in our project, and although we were unsuccessful at demonstrating mechanical cell lysis at the microscale, we have laid the groundwork for continued work in this area.

Since our two device components mentioned previously are fabricated in silicon, we also sought to develop novel methods for interfacing to the devices using plastic manifolds with dimensions on the order of hundreds of microns to millimeters. This will enable more robust testing of the devices and serve as a starting point for developing packaging strategies for surface micromachined silicon microfluidic devices.

1.0 Particle Separation and Cellular Particle Collection

After a biological sample has been collected (air sampler, or a syringe-drawn sample), the fluid sample then needs to be processed to separate relevant analytes from contaminants. Many contaminants can inhibit bioassay reactions or give false positives at the detector. Many methods exist to conduct such separation in commercially available biological detection systems, but we have utilized a new technique that employs a high frequency (~MHz) AC field to induce dielectrophoresis (DEP) and phase separation in particle fluid suspensions. This method separates cellular particles from non-cellular particles using the intrinsic polarizability properties of analytes, obviating the need for lengthy and expensive labeling steps.

1.1 Dielectrophoresis

We will consider a particle of permittivity ε_p and conductivity σ_p suspended in a fluid with permittivity ε_f and conductivity σ_f [Fig. 1]. After exposure to an electric field, a flowing particle acquires a dipole moment as it becomes polarized. Polarization is a relative shift of positive & negative electric charges in opposite directions induced by a field, and in the case where the particle and fluid have different permittivities and conductivities, charge will build up at the interface between the particle and the fluid.
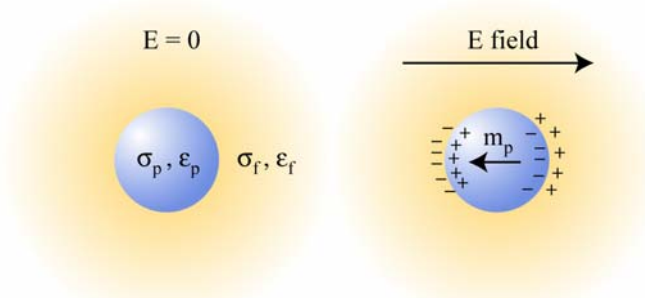
Fig. 1: Maxwell-Wagner polarization of a particle suspended in a fluid under an external electric field.

This effect is termed the Maxwell-Wagner effect, and is due to the disparity in charge flow between the two constituents with different polarizability properties [1,2]. A polarized particle subject to a spatially non-uniform electric field experiences a force, referred to as a dielectrophoretic (DEP) force [3]. The time average dielectrophoretic force in an AC field, F_{DEP}, is proportional to the product of the particle volume, v_p, the gradient of the square of the rms (root mean average) of the field strength, and the real component of the relative particle polarization, $\beta^*(\omega)$, at the field frequency ω:

$$F_{DEP} = \frac{3}{2}\varepsilon_0 \varepsilon_f v_p \, \text{Re}(\beta^*(\omega))\nabla E_{rms}^2$$

Eq. 1

$$\text{with } \beta^*(\omega) = \frac{\varepsilon_p^* - \varepsilon_f^*}{\varepsilon_p^* + 2\varepsilon_f^*} \quad \text{and } \varepsilon^* = \varepsilon - j\frac{\sigma}{\omega}$$

where ε_0 is the vacuum permittivity, $\sigma_{p/f}$ is the particle/fluid conductivity, $\varepsilon_{p/f}^*$ is the complex permittivity of the particle/fluid. The electric field must be non-uniform $(\nabla E_{rms}^2 \neq 0)$, and there must be a discontinuity in ε^* between the particle and the fluid in order for particle motion to occur. The gradient in the electric field leads to a nonsymmetrical dipole in the particle. This produces a net force on the particle
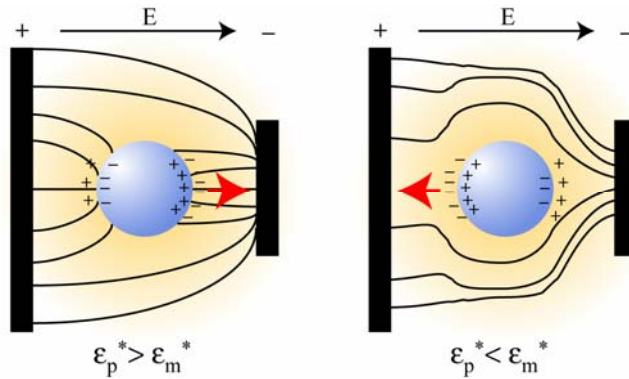
Fig. 2: Positive dielectrophoresis (left) and negative dielectrophoresis (right). Red arrows depict the particles' direction of motion.

accompanied by motion [Fig. 2]. If the particle is more polarizable than the liquid ($\text{Re}(\beta^*) > 0$), the particle will migrate towards regions of maximum ∇E_{rms}^2, termed positive dielectrophoresis (pDEP). If the particle is less polarizable than the fluid ($\text{Re}(\beta^*) < 0$), the particle will migrate towards regions of low ∇E_{rms}^2, termed negative dielectrophoresis (nDEP). This DEP effect can occur for both AC and DC voltages, and has been investigated for some time as a method for particle separation [4-7].

1.11 Effects of Surface Conductivity

In order to account for observed experimental effects of DEP, we also need to take into account the surface conductivity of particles in addition to their bulk conductivity [8]. Thus the total conductivity of a particle is given by:

$$\sigma_p = \sigma_{p,bulk} + \sigma_{p,surface} = \sigma_{p,bulk} + \frac{2\kappa_s}{r_p} \qquad \text{Eq. 2}$$

where κ_s is the particle surface conductance caused by the surface charge and double layer surrounding the particle of radius r_p. For homogeneous particles such as
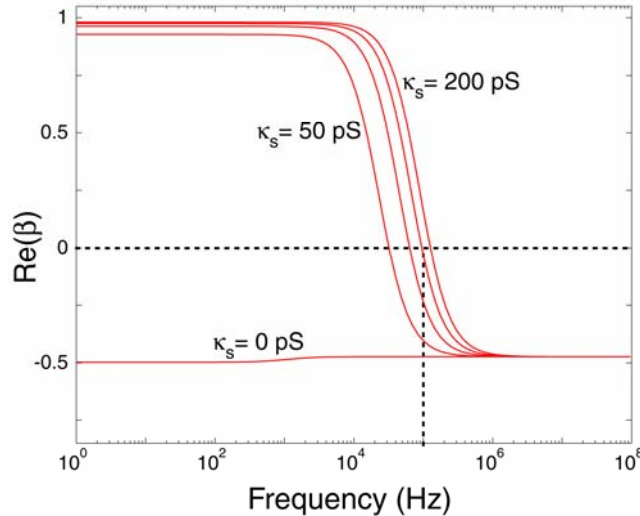
Figure 3: Theoretical plot of $\text{Re}(\beta^*)$ as a function of frequency and surface conductance.

polystyrene microspheres, we can plot $\text{Re}(\beta^*)$ as function of frequency and surface conductance Using $\varepsilon_p = 2$ and $\sigma_{p,bulk} = 1\times10^{-16}$ S/m for typical polystyrene microspheres and $\varepsilon_f = 79$ and $\sigma_f = 5\times10^{-4}$ S/m for DI water, Fig. 3 shows the predicted behavior of $\text{Re}(\beta^*)$. The limits of $\text{Re}(\beta^*)$ are between -0.5 and +1.0, and if the surface conductance on the polystyrene microspheres is 0, the particles should exhibit nDEP for all

frequencies. As surface conductance is added to the model, the behavior becomes more complicated, and the particles will display both nDEP and pDEP in different frequency ranges. The plot also indicates frequencies at which $\mathrm{Re}(\beta^*) = 0$, meaning there will be no DEP force exerted upon the particles. Another point to note is that at higher frequencies ($>10^6$ Hz) the surface effects are eliminated, and surface conductance has no effect on the DEP response of the particle. This can be used advantageously to separate particles based on their bulk properties, while ignoring surface characteristics.

We measured the complex permittivity of polystyrene particles suspended in water using an Agilent Model 8753ES Vector Network Analyzer. We used a low field (V/mm), and by measuring the permittivity for different volume fractions (ϕ) ranging from 0.1% to 10% (v/v), we were able to calculate the value of $\mathrm{Re}(\beta_s^*)$, which is the relative polarizability of the *particle suspension*, as a function of frequency. Using the following:

$$\beta_s(\omega) = \frac{\varepsilon_s^* - \varepsilon_m^*}{\varepsilon_s^* + 2\varepsilon_m^*}, \quad \beta(\omega) = \left(\frac{1}{\phi}\right)\beta_s(\omega) \qquad \text{Eq. 3}$$

we can then calculate $\mathrm{Re}(\beta^*)$, the relative polarizability of the *particles*. Figure 4 shows the real and imaginary components of both the particle suspension and the particles. In the frequency range in which we are operating (1-30 MHz), the polystyrene particles
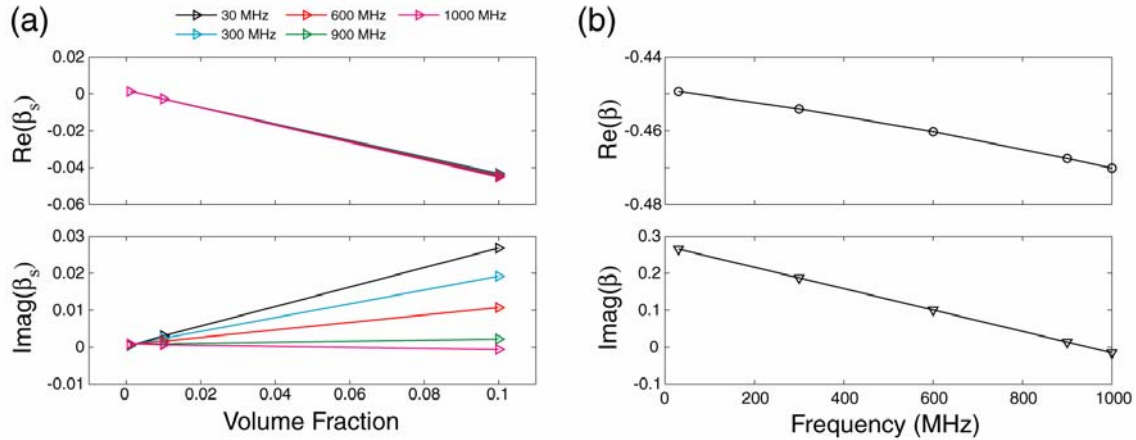
Figure 4: (a) Plots of the real (top) and imaginary (bottom) components of the complex permittivity of the particle suspension as a function of volume fraction (v/v) and frequency. (b) Plots of the real (top) and imaginary (bottom) components of the complex permittivity of the particles as a function of frequency.

suspended in water will exhibit very strong nDEP ($\mathrm{Re}(\beta^*) \sim -0.5$). The frequency limitations of the measurement apparatus prevented the determination of the polarizability of the particles at lower frequencies.
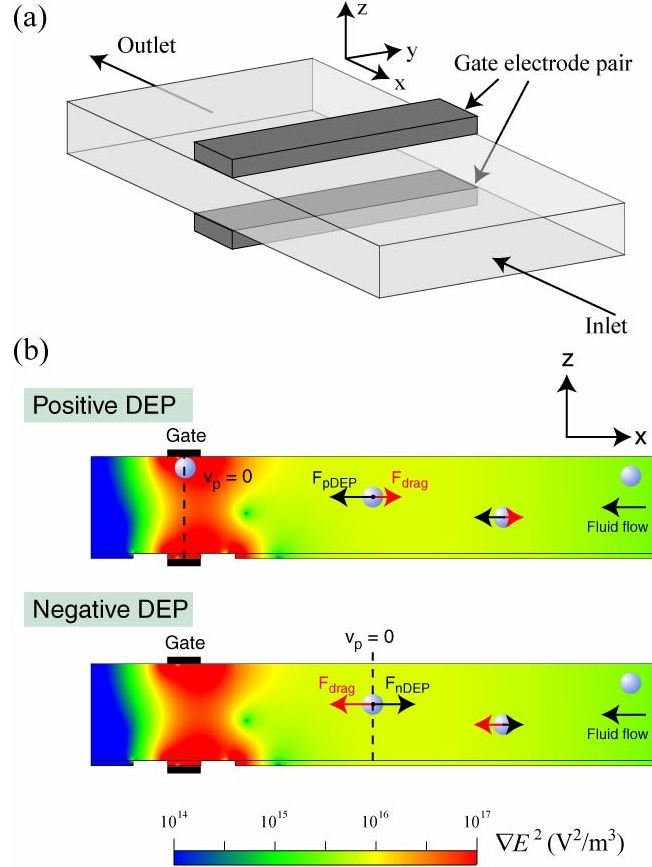
Fig. 5: (a) Schematic of a dielectrophoretic gate consisting of two electrodes arranged perpendicular to the fluid flow. (b) The field distribution of the gradient of an AC field $(\nabla E_{rms}^2(x,z))$ **near the gate, and the forces acting on negatively and positively polarized particles. Electrodes (black rectangles) are added for clarity.**

1.2 Dielectrophoretic Gate

In conjunction with our colleagues from the New Jersey Institute of Technology, City College of New York, and NASA, we have developed and demonstrated a new concept for the electro-separation of bio-particles from non-biological materials, termed "*dielectrophoretic gating,*" a technique that combines the field-induced dielectrophoresis and phase transition for manipulating particles in micro-fluidics [9,10]. To form a dielectrophoretic gate, microelectrodes are arranged within a fluidic channel so as to create a highly localized gradient of the AC field strength perpendicular to the flow. Figure 5a shows a two-dimensional simulation (CFD-ACE+ Version 2003.0.136) of the dielectrophoretic gate. The grid density was 10 points per μm, and the electrodes were set to 10 volts. In this simulation, the height of the channel was $7\,\mu$m, and the electrode surfaces were 2 μm wide. The topography at the electrode edges was neglected, and all other surfaces were set to the boundary condition of zero normal current. The field

gradient is largest at close distances to the microelectrodes and, in this example, ∇E^2_{rms} maintains a value of $\sim 10^{17}$ V^2/m^3 or greater throughout the z-axis near the gate. The range of $\boldsymbol{F}_{DEP}$ operating along the flow streamlines was extended throughout the height (z-axis) of the channel by placing an electrode on the top and bottom surfaces of the channel. This helps to increase the gating efficiency in that particles suspended in a fluid flowing at any position in the yz plane have a higher probability of being subjected to $\mathbf{F}_{DEP}$.

Upon injecting a solution of analytes that are more polarizable than the suspending fluid, the analytes will accelerate under pDEP towards the regions of highest ∇E^2_{rms}, which is near the microelectrodes (Fig. 5a). Solving the equation of motion for a particle by taking into account $\boldsymbol{F}_{DEP}$ and the drag force while neglecting the interparticle interactions and the gravity force, the velocity $\boldsymbol{u}$ of a small spherical particle of radius r_p traveling in a flowing fluid is given by [11, 12]:

$$\boldsymbol{u} = \boldsymbol{v} + \frac{\boldsymbol{F}_{DEP}}{6\pi\eta r_p} \qquad\qquad \text{Eq. 4}$$

where η and $\boldsymbol{v}$ are the fluid viscosity and velocity, respectively. For large ∇E^2_{rms}, $\boldsymbol{F}_{DEP}$ will attract highly polarizable analytes to the microelectrodes where they will come to rest. In contrast, for analytes that are less polarizable than the fluid, $\boldsymbol{F}_{DEP}$ will act as a repulsive force as the analytes seek to migrate toward regions of low ∇E^2_{rms} (Fig. 5b). Thus, if the particles injected into the channel have low polarizability, they will be carried with the fluid flow until the value of ∇E^2_{rms} reaches the point at which the particles start being subjected to nDEP. This force will then decelerate the particles, producing a drag force as the particle motion begins to oppose the fluid motion, and, at some location upstream from the gate, the particles will come to rest at the point where $\boldsymbol{F}_{DEP}$ equals the drag force. A larger fluid velocity will push the particles closer to the gate, while a smaller fluid velocity will allow the particles to be repelled at greater distances from the gate. Upon injection of a mixture of low- and high-polarizability particles, the opposing nDEP and pDEP forces will separate the particles rapidly.

1.3 Fabrication of the Dielectrophoretic Gate

The devices were fabricated at the SNL Microelectronics Development Laboratory. The dielectrophoretic gate we present here was fabricated using a previously described process termed SwIFT™ (Surface Micromachining with Integrated Fluidic Technology) [13]. SwIFT™ is a sacrificial layer method that uses multiple layers of structural materials (polysilicon and silicon nitride) and sacrificial materials (silicon oxide) to build devices. The SwIFT^{TM} process begins with six-inch bare (100) n-type wafers with 2 – 20 Ω-cm resistivity (Fig. 6a). Next, the bulk silicon is isolated from the devices with a 0.6 μm layer of thermally grown silicon oxide followed by a 0.8 μm layer of non-stoichiometric (silicon-rich) low-stress silicon nitride (N0). Up to five layers of fine-grained doped polysilicon (P0-P4) are deposited from silane in a low-pressure
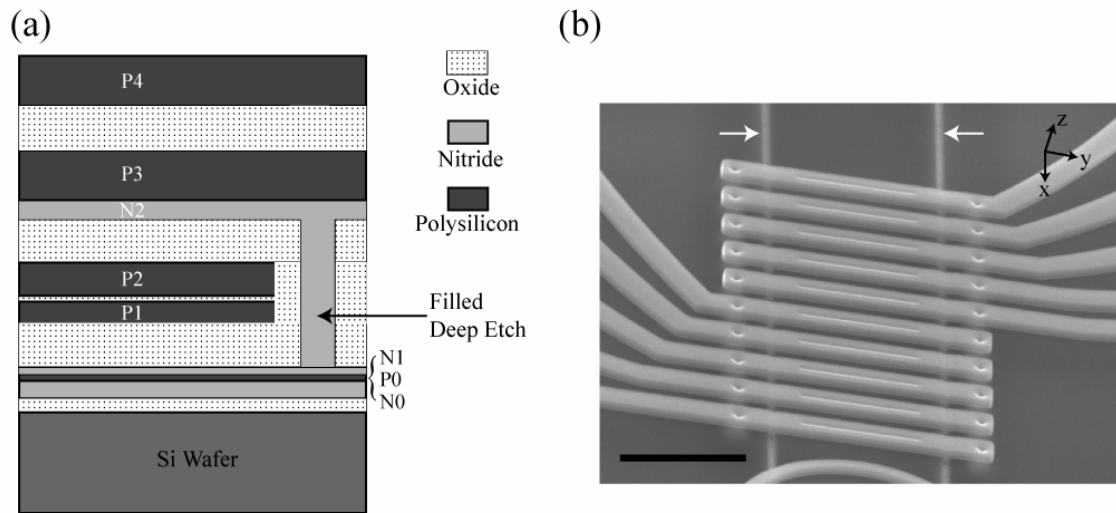
Fig. 6: (a) SwIFT™ film stack with five polysilicon, three silicon nitride, and four sacrificial silicon oxide layers. (b) Scanning electron micrograph of a series of dielectrophoretic gates. The fluid channel sidewalls are noted (white arrows). Scale bar = 30 μm.

chemical vapor deposition furnace. These layers are used for making electrical connections and microelectrodes in order to impart electric fields into microfluidic compartments. Polysilicon layers are on the order of 1-2 μm thick, with the exception of P0, which is 0.3 μm. The sacrificial oxide layers are deposited using both low pressure chemical vapor deposition and plasma enhanced chemical vapor deposition. Chemical-mechanical polishing is used to reduce the topography in the final two sacrificial oxide layers. The structural layers of silicon nitride (N1: 0.3 μm, N2: 0.8 μm thick) provide optically transparent and electrically insulating surfaces that serve as barriers for the fluidic components. Figure 6a indicates a deep etch through several sacrificial oxide films down to N1. This trench is then filled with N2, forming sidewalls and ceiling covers for fluidic channel components. The total film thickness is 16 μm, and the distance between N1 and N2 is ~7 μm. Figure 6b shows a close-up image of a completed device with 10 sequential DEP gates. The N2 channel sidewalls are visible, along with the P3 electrode traces perpendicular to the fluid channel axis. P4 was not utilized in this particular device. The circular depressions are vias that connect the P3 microelectrodes to the P0 microelectrodes (not visible), allowing them to be held at the same potential. The long depressions in the center of the P3 traces are due to etches in N2 that allow the P3 microelectrode to be in direct contact with the fluid flowing through the channel. Similar etches are made in N1 to allow P0 to contact the fluid.

After completing the surface micromachining, access ports to the fluidic devices are fabricated using deep reactive ion etching [14]. The sacrificial oxide layers in devices are then removed in an HF-based etchant at 20° C for 100-200 minutes depending on the
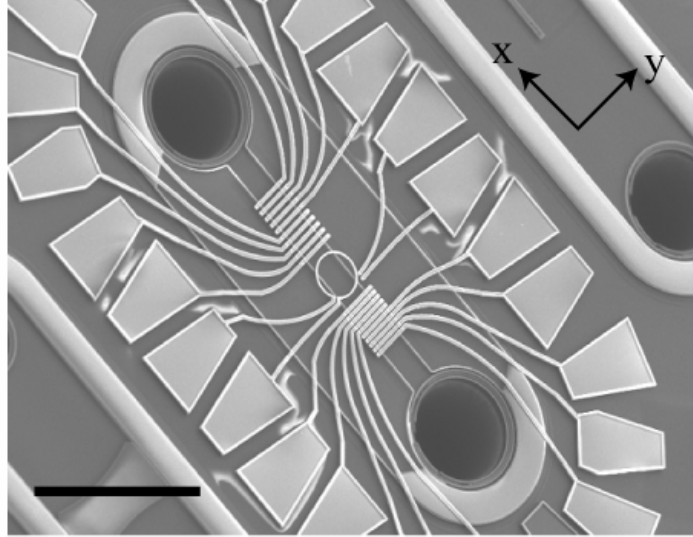
Figure 7: Completed microfluidic device using the SwIFT^{TM} technology. Scale bar = 150 μm.

length of the fluidic channel. The devices are then rinsed in deionized (DI) water and dried in supercritical CO_2. Figure 7 shows a completed fluidic device with integrated dielectrophoretic gates. The channels are fabricated in a fully encapsulated state, obviating the need for substrate bonding, a process that slows the device production and reduces reproducibility. The bulk silicon etches forming the inlet and outlet of the channel are visible, in addition to bond pads for introducing voltages to the microelectrodes.

1.4 Polarizability of particles in the radio frequency range

In the radio frequency (RF) range (0.1-30 MHz), the relative polarizability of a low conductivity particle immersed in water is mainly influenced by the ratio of capacitances of the particle and the water, so that $\mathrm{Re}(\beta^*)$ is given by:

$$\mathrm{Re}(\beta^*) \approx \frac{\varepsilon_p - \varepsilon_f}{\varepsilon_p + 2\varepsilon_f} \qquad \text{Eq. 5}$$

where ε_p and ε_f are the dielectric constants of the particle and the suspending fluid, respectively. The dielectric constant of water at radio frequencies is about 80. In contrast, dielectric constants of soil components and common industrial and natural materials (for example, resins, plastics, carbon black, soot, fly ash, gravel, cement powder, gypsum, insulation, press board, sand, wood, salt, sugar, glass, quartz, oils, paper, carbon black, flour, powdered milk, cereal, corn, popcorn, seeds) when dry fall in the range, 1.5 to 15. In particular, the fact that dielectric constants of common materials are significantly smaller than that of water is routinely used for the radar monitoring of the water content of soil, vegetation, snow, agricultural products, and many industrial materials. Since the particle polarization in the radio frequency range is mainly specified by its bulk dielectric
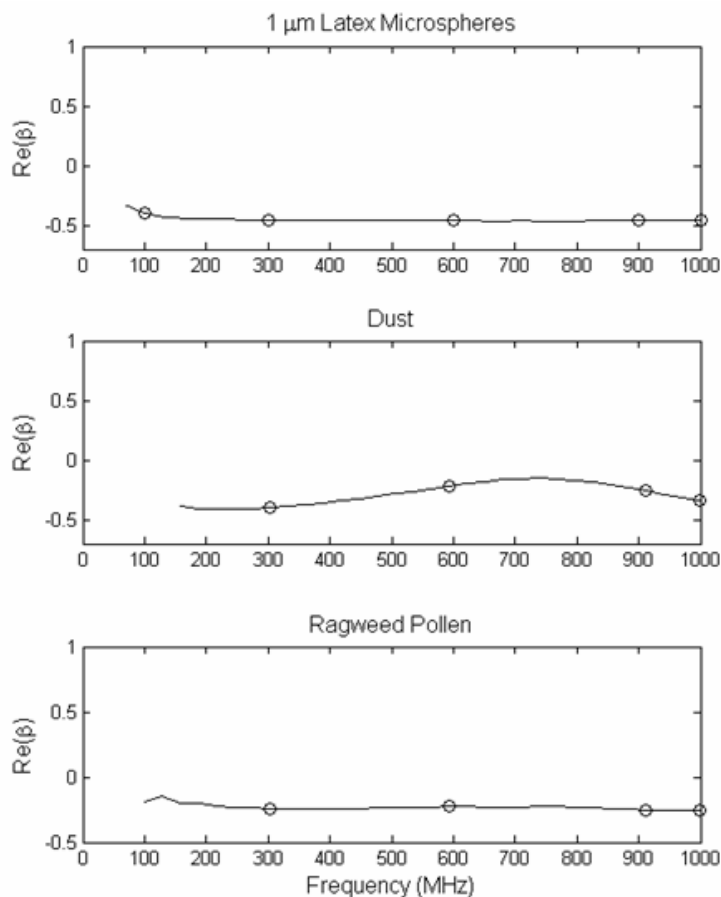
Figure 8: *Re(β)* as a function of frequency for several particles.

constant, all these materials when dispersed in water will exhibit strong negative dielectrophoresis until they become saturated with water. Figure 8 shows the measured *Re(β)* for several particles suspended in DI water: latex microspheres (1 μm diameter), Arizona test dust (0.6-20.0 μm diameter particles; mostly SiO_2 and Al_2O_3), and ragweed pollen (20-24 μm diameter). All three of these particles exhibit $\mathrm{Re}(\beta^*) < 0$, and would thus undergo nDEP in DI water. Potential biological contaminants such as weed pollen require further study to determine their DEP behavior in comparison to biological targets such as smaller bacterial cells and spores.

An exception to the assumption that most non-cellular particles will undergo nDEP in the MHz frequencies can occur when the particle has a high conductivity, such as glassy carbon ($\sigma \sim 10^4$ S/m) or metal particles ($\sigma \sim 10^6$ S/m). When we calculate $\mathrm{Re}(\beta^*)$ using these parameters (Fig. 3), these types of particles are predicted to undergo pDEP in the RF range. We are planning to conduct experiments to examine the separation of cells from highly conductive non-cellular particles, with the intent on exploiting either the frequency dependence of the polarization or the density disparity between metal particles($\rho > 1$ g/cm^3) and cells ($\rho \sim 1$ g/cm^3).

1.5 Field-induced DEP and phase transition for separating biological and non-biological particles

Separation of bio-particles from non-biological materials in our device is accomplished by employing an AC field in the radio frequency range within which typical airborne particles of non-biological origin appear to be less polarizable than water so that they undergo nDEP and are repelled from the gate. In contrast, biological particles whose polarizability in the MHz-frequency range appears to be close to that of water will flow through the gate. Another essential advantage of this frequency range is that undesirable electric effects in water, such as electrolysis, electro-osmosis, and electro-
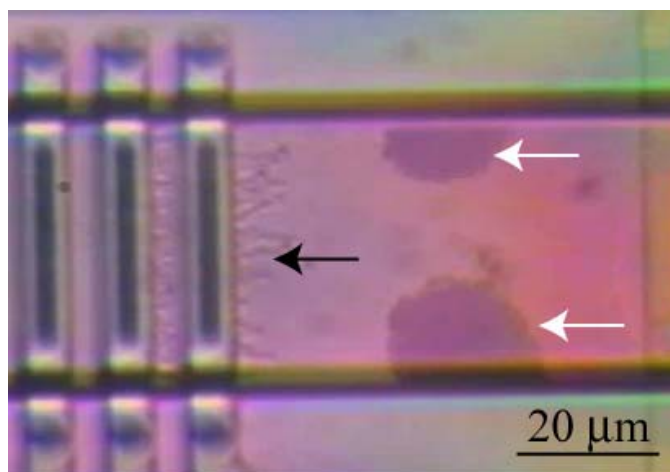
Fig. 9: Positively polarized bacteria accumulate at the gate (black arrow), while negatively polarized latex particles accumulate upstream from the gate (white arrows).

convection are suppressed, that makes it particularly well suited for microfluidic applications. Since electrophoretic effects also vanish at MHz-frequencies, this technique employs bulk polarization properties of a particle, given by $\mathrm{Re}(\beta^*)$, that are insensitive to the particle surface properties which may vary due to environmental effects or intentionally in the course of the aerosol fabrication.

Figure 9 shows the separation of a mixture of $1\,\mu\mathrm{m}$ latex particles from dead Staphylococcus aureus bacteria. The gate was set to 10 volts peak-to-peak at 15 MHz. The positively-polarized bacteria accumulate at the gate microelectrode, while the negatively-polarized latex particles are repelled from the gate region. As the bacteria accumulate at the gate, the polarization interactions occur and long pearl-chains of bacteria form that exceed the bounds of the gate. At high fluid velocities (~50 μm/s), the latex particles formed fronts close to the gate and the interparticle interactions became more apparent. In particular, at a fluid velocity of ~45 μm/s (flow rate ~ 6 pL/s) the repelled latex particles aggregated at $x \sim 25$ μm upstream from the center of the gate (Fig. 9) with the average particle concentration in the aggregate running as high as 40-50% (v/v). The particle aggregate oscillated between forming one bolus being located in the center of the channel and two rotating boluses being located at the channel sidewalls.

Figure 10 documents that switching the gate frequency from 15 MHz to 100 kHz causes the rotating boluses adjacent to the channel sidewalls to traverse the gate, while the bacteria remain trapped. At an estimated fluid velocity of 45 μm/s, all the accumulated latex particles escape the gate within about 5 s following this frequency shift. However, the pDEP force on the bacteria at this frequency is still strong enough to withstand the fluid flow. This release of the latex particles is related to the reduction of their relative polarizability, $\text{Re}(\beta^*)$, with decreasing field frequency, as was observed in [15] under similar conditions, and as predicted by the previous discussion (Fig. 3).

A low injection fluid velocity was used to isolate the DEP-induced velocity on the bacteria. Upon injection of the mixture, the fluid velocity was measured to be 5-10 μm/s,
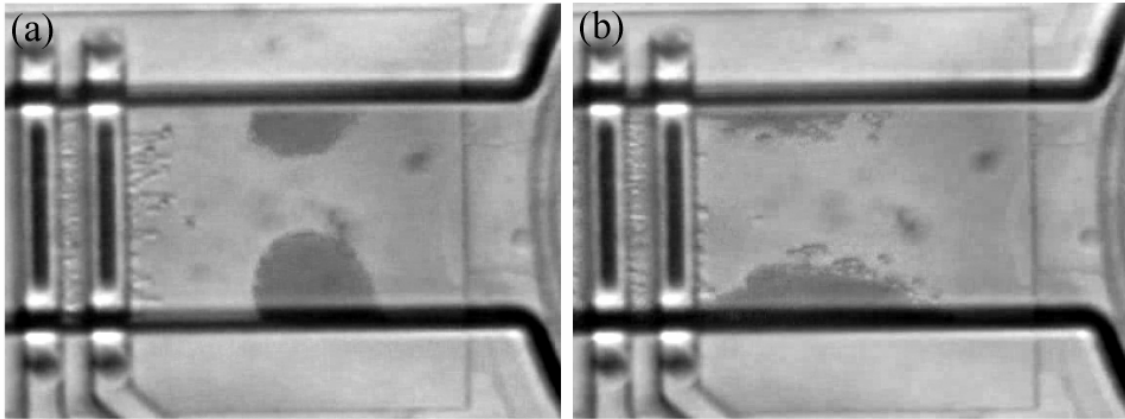
Figure 10:(a) DEP gate held at 10 V, 15 MHz. (b) DEP gate switched to 100 kHz, allowing the latex particles to escape the gate.

and at this velocity, the latex particles formed a distinct front ~40 μm upstream from the gate. Three individual bacteria had their distance-dependent velocities, $u(x)$, tracked from their entrance into the channel until they came to rest at the tips of pearl chains 5 μm upstream from the gate (Fig. 11). The fluid velocity was kept low (5-10 μm/s) which was much smaller than the DEP-induced particle velocity. The large DEP-induced particle velocities made it difficult to track bacteria within 20 μm of the gates, hence the velocity data were fitted to an exponential curve [$u\,(\text{in}\,\mu m/s) = 1330 e^{-0.122x}$, x in μm, with $r^2 = 0.92$] to provide an estimate of the particle velocities generated near the gate. Thus, it was found that the bacteria were accelerated to velocities up to ~700 μm/s before coming to rest adjacent to the gate. Using Eq. (4), the maximum estimated forces exerted on individual bacteria are on the order of 5 pN. Figure 11 also shows the velocity data of four latex particles that were tracked while undergoing nDEP. In addition, the fluid velocity was increased in order to examine the strength of the repulsive force. It was found that, after the latex particles were injected at velocities of 75-100 μm/s, the DEP force started to exert an observable deceleration of particles at $x \sim 30$ μm from the gate, with full repulsion bringing particles to a halt ~12 μm upstream from the gate. Latex

particles flowing at velocities of up to ~600 mm/s have been prevented from traversing the gate using a 10 V p-p, 15 MHz excitation voltage.

Accumulated downstream from the front of the gate (Fig. 9), negatively polarized non-biological particles interact with one another through dipole-dipole forces due to their polarization. When the amount of the accumulated particles exceeds the threshold value, these interactions cause the suspension to undergo the phase transition and separate into low- and high-concentrated phases by rearranging the particles into aggregation patterns, often referred to as the electro-rheological effect [16], and forming a distinct front (the boluses in Fig. 9) between the regions enriched with and depleted of particles, the average particle concentration in this location runs as high as 40-50% (v/v). By reversing the flow, the boluses can easily be removed from the channel.
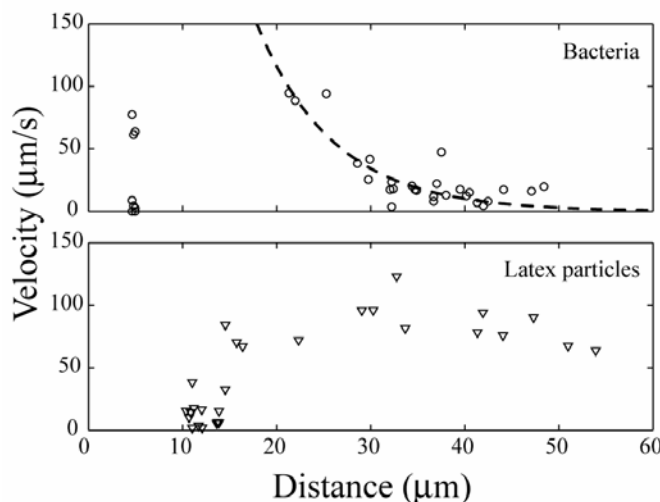
Figure 11: DEP-induced velocity of bacteria (top) and latex particles (bottom).

The evolution of the particle patterns formation is well described by a proposed electro-hydrodynamic model which does not require any fitting parameters [9, 17]. This three-dimensional model encompasses the quasi-steady electrodynamic equations coupled with the momentum and continuity balance equations of the "mixture" model for a suspension. Further discussion of this model is outside the scope of this report.

2.0 Cell Lysis Devices

Identification techniques in biodetection require access to the genetic material within cells and viruses. Many cells are encapsulated in rigid cell wells or fluid lipid membranes. There are many techniques used to lyse cells such as ultrasonication, chemical methods, and electrical methods. Ultrasonication methods typically require the addition of large microspheres (100 μm diameter) to help generate enough force to rupture membranes and cell walls, making this a difficult technique to scale down and implement in a microdevice. Chemical methods require extensive buffer exchange in order to deliver and then remove the lysing chemicals from the environment before DNA amplification since many of the chemicals can interfere and inhibit nucleic acid amplification. These methods have been miniaturized, but there are difficulties in scaling

down to single cell analysis microsystems. Electrical methods work well and can be scaled down, but concerns about localized heating and electrochemical reactions occurring at microelectrode interfaces have limited the use of this method.

We have pursued mechanical lysis within a microsystem for several reasons. Mechanical lysis is much cleaner in the sense that chemicals are not required, and voltages are not directly imparted to the fluid, generating heat and electrochemical reactions. There are mechanical methods currently available for lysing cells such as French presses and specialized blenders, but they are large systems that don't work well with small numbers of cells. One advantage of mechanical lysis is that we can fabricate micro-scale mechanical pistons that can to lyse single cells one at a time. One of the
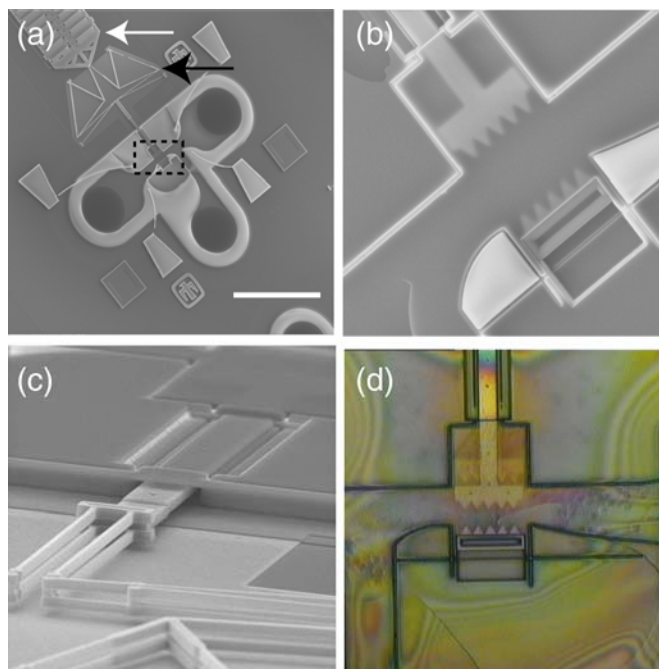
Figure 12: Mechanical cell lysis device. (a) Electrostatic comb drive (white arrow), displacement multipler (black arrow), and the active lysis region (black square) are noted. Scale bar = 125 μm. (b) Close up of the active region. (c) Side view of the mechanical piston's entrance into the fluidic channel. (d) Image of red blood cells passing through the device.

disadvantages is that most cells are fairly flexible, and may simply deform under mechanical stress rather than rupture. To our knowledge, this is the first attempt at mechanical cell lysis at the microscale.

We are currently testing cell-lysis devices for optimization of certain factors such as mechanical stroke distance and frequency of operation. Recent devices contain mechanical pistons that can also be used to apply electrical potentials, adding an electrical component for rupturing the cells in addition to mechanical shear. The most recent designs contain hollow pistons for transfection of cells or removal of genetic material from the cell. We have also sought to increase the mechanical force by replacing high-performance electrostatic comb-drives, which have been predicted to provide

hundreds of micronewtons of force, with thermal actuators that are capable of millinewtons of force.


2.1 Fabrication of the Mechanical Cell Lysis Devices

Section 1.3 details the SwIFT^{TM} process that was used to fabricate the cell lysis devices. Similar layers were used, except an additional "dimple cut" layer was used in these mechanical devices to provide extra clearance for the moving piston. Figure 12 shows images of a completed device. The device contains three inlet/outlet ports. The third chemical entry/extraction port can be used to make this device operate in a continuous flow system. Such a device would enable injection of genetic material, proteins, and fluorescent tags into the cells and in a massively parallel setup large numbers of cells can be processed. Polysilicon electrodes are also incorporated into this device to allow additional manipulations and measurements such as electroporation, extracellular recordings, and field-assisted vesicle fusion.

This particular device was powered by an electrostatic comb-drive. A displacement multiplier was also incorporated to increase the throw of the piston by 12X. The piston contains sharp edges that abut to an opposing set of stationary edges (Fig. 12b). The first set of devices were sub-optimal in that the opposing edges remained too far apart at the maximum throw of the piston, preventing large shear forces from being imposed on traversing cells. Another difficulty with the device is the entrance of the piston into the fluid channel. This leaves a small opening through which fluid can leak, causing losses in sample volume (Fig. 12c). The sample loss can be kept to a minimum be sealing the entrance with high viscosity silicone oil that won't breach the entrance and will keep aqueous solutions form exiting.

In one experiment, a dilute solution of red blood cells was pumped through the device using a syringe with the manipulator running (Fig. 12d). Smooth, sub-Hz mechanical actuation of the cell disrupter was observed as well as actuation in the kHz range using 10-30 V voltages. The cellular membranes were observed to deform significantly on contact with the disrupter, but no visible evidence of lysis was observed.

Newer designs have addressed several issues found in testing of the first-generation devices. The piston assembly was reconfigured to allow it to make contact with the stationary edges to increase the shear force generated on the cells. A second generation of this device has also been fabricated that contains hollow structures for allowing direct injection/withdrawal of materials into/from cells. We have also incorporated thermal actuators, which have the potential of generating forces up to 10s of mN, into these devices. A dilute suspension of yeast cells were introduced into a device with a thermal actuator (Fig. 13). Fluorescein dye was added to the cell suspension in order to help visualize cell deformation within the active region of the device. This experiment documents the mechanical deformation of a single yeast cell, with the deformation being held for several seconds (Fig. 13b) before release of the actuator allows the cell to return to its original shape (Fig. 13c).
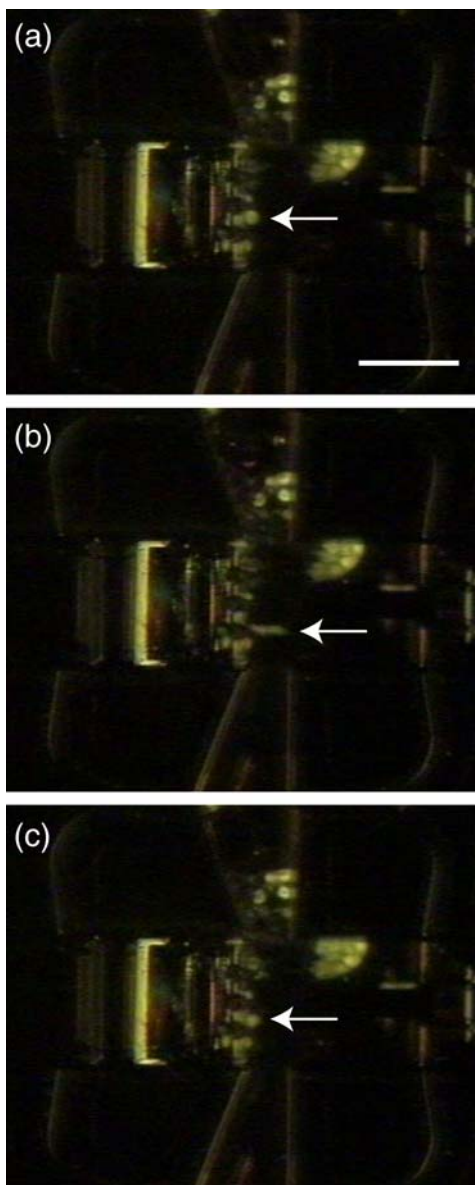
Figure 13: Deformation of a single yeast cell (arrow). (a) t = 0 s. Scale bar = 25 μm. (b) t = 0.3 s. (c) t = 3.9 s.

3.0 Polymerase Chain Reaction Approach and Results

After cell lysis, we will need to quantitate the amount of DNA that can be extracted and detected from the small volumes of material expected from lysing single cells. We will test the limits of amplifying and detecting genetic material using a conventional PCR apparatus interfaced with our micro- cell lysis device. We have acquired a real-time PCR system (Applied Biosystems) for detecting minute quantities of DNA. Real time PCR is the fastest, most sensitive, and smallest volume DNA identification system available currently. We have determined how well the amplification occurs on nucleotide sequences immobilized to latex microparticles.

Conventional PCR is typically performed in 50ul volumes, however the output of the DNA isolated from our proposed microdevice is expected to be much smaller (~ 1μL). To test the limits of the PCR system interfaced with our devices, we will amplify a single, known sequence of DNA. We will test various concentrations of the DNA in various volumes with the goal of achieving successful PCR in 10-20ul volumes. Once conditions have been optimized for small volumes, these conditions will be used to test DNA that has been captured in the microdevice. Our objective was to use PCR to detect DNA that has been isolated from a single cell via the capturing, lysing and separation capabilities of the dielectrophoretic channel.

The tagged particles will provide the surface area and specificity for capturing minute quantities of antigens, DNA/RNA molecules, and internal protein markers. The particles, being large in comparison to the molecules, can then be collected and separated, before being sent off to analysis. Finally, real-time polymerase chain reaction (PCR) with a commercially available system will be interfaced with our microdevice in the first step of genetic identification of a particular agent.

3.1 System Design and Experiments

Custom synthetic oligos were purchased from Integrated DNA Technologies, Inc. The oligos were designed to be attached to beads and subsequently amplified by PCR. A 100-mer strand and its complement and two primer sequences were used. The 100-mer strand was modified at the 5' end with a biotin molecule separated from the sequence by a 15-atom carbon spacer. The 5' end of this strand was attached to paramagnetic beads and the spacer was thus necessary to reduce the proximity of the oligo to the bead so that the PCR molecules would have access to the sequence. Using standard protocols the biotinylated 100-mer was annealed to its complement prior to its binding to the beads.
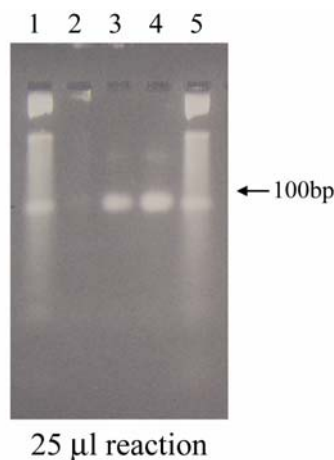
Figure 14: Agarose gel results for a 25 μl reaction volume. Lane 2 (oligo attached to beads), lane 3 (free oligo with beads added to the reaction), lane 4 (oligo only), lane 1 and 5 (10 bp DNA ladder).

The primers were designed to amplify a 70 base pair sequence of the 100-mer. The sequences were:

100mer Oligo:
5'/BioTEG/TATTCGGTACTTCAACAAATGGATATCTTGAGTTGCTTCGACAATG
AGATAGCAGTTCCAAATATGACCACGGAATAGATCTTGATGAGTTAAACAGA
TT-3'

Complement:
5'ATAAGCCATGAAGTTGTTTACCTATAGAsACTCAACGAAGCTGTTACTCTAT
CGTCAAGGTTTATACTGGTGCCTTATCTAGAACTACTCAATTTGTCTAA-3'

Forward Primer:
5'TGGATATCTTGAGTTGCTTCGAC-3'

Reverse Primer:
5'CTCATCAAGATCTATTCCGTGGTC-3'

Streptavadin coated, paramagnetic beads (1.5 µm diameter) were purchased from Bangs Laboratories, Inc. The beads were washed twice in PBS then 1000 picomoles of biotinylated double stranded oligo were conjugated to 200ul of the beads by incubating in PBS for 15 minutes at room temperature. The beads were magnetically separated and any unbound oligo was washed away. Two µl of the conjugated bead/oligo were used in PCR amplification. 25 µl and 50 µl reactions were tested. PCR on unbound DNA was used as a positive control. PCR was done using PCR SuperMix from Invitrogen Corporation in the following solution:

	25 µl Reaction	50 µl Reaction
Bead/oligo	2 µl	2 µl
1.1x Supermix	20 µl	43 µl
Forward Primer	1.5 µl	2.5 µl
Reverse Primer	1.5 µl	2.5 µl

Table 1: PCR solution used in bead immobilized amplification of DNA.

Figure 14 shows the results of a successful 25 µl reaction of DNA bound to microspheres (Lane 2). Lanes 1 and 5 are DNA ladder standards used to compare sample size. Lanes 3 and 4 are controls which show amplification of our target when it is not bound to the microsphere surface. Comparing these lanes to lane 2, the case of microsphere bound targets, we see that the amplification reaction is somewhat inhibited by the target being bound to the surface. Further exploration of the spacer length will be required to optimize the amplification of microsphere bound DNA.

4.0 Polymer Manifolds for Silicon Microfluidic Devices

In order to rapidly handle a large (by surface micromachining standards) fluid sample volume of 1 µl to 1 ml in a surface micromachined microfluidic device, a parallel flow circuit is needed. This will enable high throughput applications for our devices, as well as provide some of the infrastructure that needs to be developed for robust packaging. The meso-scale microfluidic package (flow manifold) moves the fluid from an input port to an input channel that feeds several (potentially 100's or even 1000's – but on the order of 2 to 10 initially) surface micromachined microfluidic channels
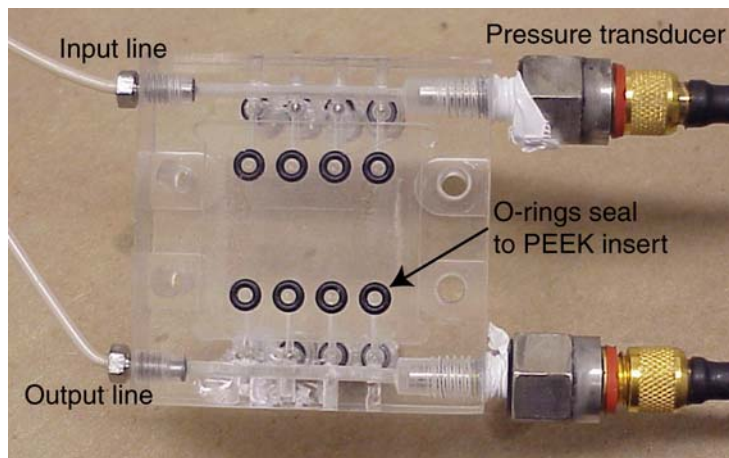

Figure 15: Front view of flow manifold with PEEK insert and silicon die removed.

each containing the necessary microfluidic components. In the case of a cellular sample pretreatment system these components would include a dielectrophoretic trap for pre-lysing separations, followed by a device to lyse the cells, followed by a 2nd dielectrophoretic trap for post-lysing separations. The effluent from the surface micromachined part of the device would then be collected in the downstream part of the meso-scale flow manifold. The sample volume would have been split into sub-volumes at this point, each containing the different constituents that have been separated from each other.

We have made some progress on the flow manifold. The flow manifold consists of an acrylic part (poly-ethyl ethylene ketone, PEEK) with 8 fluid connections allowing 4 inputs and 4 outputs to go to the silicon microfluidic die (Fig. 15). The inputs to the manifold are from upstream and downstream reservoirs through a very small dead volume capillary connector. The manifold has 2 built-in pressure transducers allowing pressure to be monitored for flow control just upstream and just downstream of the surface micromachined microfluidic chip. The inputs and outputs are controlled by applying pressure or vacuum to upstream and downstream fluid reservoirs. In addition, built-in meso-scale valves allow flow control in the manifold. The PEEK insert connects the channels in the flow manifold to the Bosch etched holes on the back of the silicon die that feed surface micromachined channels on the front. The die is attached to the PEEK manifold using double sided tape and aligned to the PEEK connecting holes using a flip-chip bonder. Further development of the system shown in the figure should allow a

sample volume to be controllably fed into an input channel feeding several microfluidic channels on a chip and then controllably withdrawn from the chip.

We have also utilized an industrial partner to develop a fluidic interface for silicon-based surface micromachined devices (Fig. 16). The manifolds were made from stacked layers (9 layers, total 41 mils thick) of polymer, with integrated fittings. A pressure-dependent bonding layer was used to interface the backside of the silicon wafer to the manifold. We are currently conducting tests looking at the strength of the seal between the silicon substrate and the pressure sensitive bonding layer. One of primary
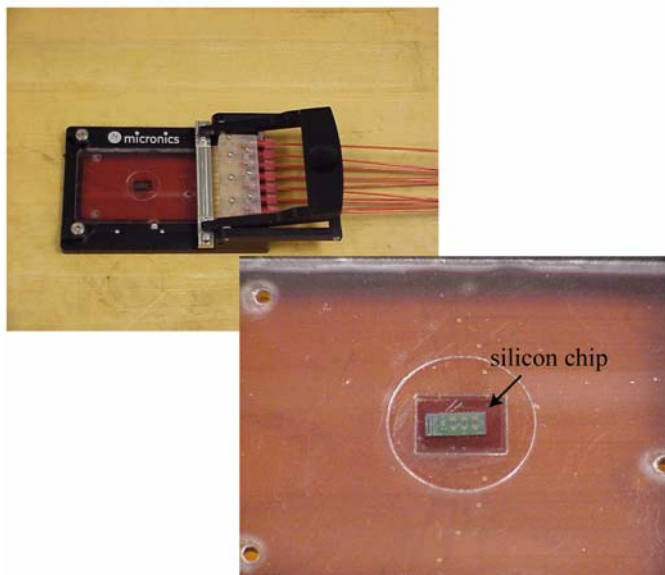
Figure 16: Manifold for interfacing to silicon microfludic devices. (Micronix)

concerns for the interface is maintaining a good seal to the device despite the fact that there are small gaps (500 μm) between adjacent inlet/outlets. These small gaps are difficult to seal over the surface area of an entire chip (8mm X 3mm). We are also examining using different configurations for the back side etch to maximize the spacing between orifices on the backside of the chip, while maintaining the fluid channel dimensions constant on the front-surface of the chip.

Conclusion

This LDRD has been successful in developing new strategies for microsystem based biological detection solutions. On the objective of sample pretreatment, we have developed a surface-micromachined dielectrophoretic gate for separating μm-sized analytes based on their intrinsic polarizability properties and validated experimentally basic relations for estimating the gate performance. The separation technique uses AC dielectrophoresis (DEP) along the flow streamlines accompanied by the field-induced phase separation through electrical and hydrodynamic interparticle interactions. The self-sealed microfluidic devices were fabricated using a surface- and bulk-micromachining technology which is amendable to mass-production. Setting the device to a moderate

voltage in the radio frequency range selectively removed bacteria cells from a mixture containing non-biological particles. The low aspect-ratio of the device permitted a high efficiency separation due to the fact that the range of the dielectrophoretic force extended throughout the cross-section of the fluid channel. This reduces the number of particles that escape the trap, producing highly concentrated (by factor over 500 the initial concentration) and spatially separated aggregates of negatively- and positively-polarizable analytes. We see a potential use for the proposed technology for discriminating between biological and non-biological analytes.

The second objective of our project was to develop a mechanical method for cell lysis. We made progress on this goal, but did not successfully demonstrate cell lysis. Through redesign of the devices, we have improved the throw and force of the mechanical actuators, and improved the ability of the devices to distort cell membranes. Further work on this objective will be pursued in the future.

We have also developed methods for interfacing to our silicon surface-micromachined devices using polymeric manifolds. Continued work in the development of microfluidics infrastructure for packaging and assembly of devices into systems will increase the likelihood of commercial use of the technology.

One of our main objectives was to develop a system capable of handling all biological threats (cell, virus, toxin molecule). Our plan was to use DEP to collect cells from a raw sample, and then to use microspheres as "capture-and-carry" chaperones for toxin molecules and viruses within the sample. This microsphere strategy would also be used to collect genetic material from cells that are lysed and viruses that are solublized. Once targets are bound to microspheres, DEP can be used to collect, sort, and concentrate the carrier microspheres. The DEP gate described here can be used for such techniques, and will require further study to determine strategies for sorting. Using a commercial PCR system, DNA bound to microspheres was successfully amplified, giving further support for our goal of using microspheres as capture-and-carry chaperones for small molecules. The results indicate that the amplification reaction is somewhat inhibited by the attachment to the microspheres, but we still maintained a reasonable level of target production. We have also validated that the typical sample volumes (1 µl) that can be produced by our sample treatment devices can be used with commercial PCR systems to amplify DNA.

References

1. Maxwell, J.C., 1873, "A treatise on electricity and magnetism," 3rd ed., Vol. 1, Ch. IX, Clarendon Press, Oxford.
2. Wagner, K.W., 1914, Archive Electrotechnik, **3**, pg. 83.
3. P.R.C. Gaskoyne and J. Vykoukal, 2002, "Particle separation by dielectrophoresis (*Review*)", Electrophoresis **23**, pp. 1973-1983.
4. Yang, L., Ruan, C., Li, Y., 2003, "Detection of viable *Salmonella typhimurium* by impedance measurement of electrode capacitance and medium resistance," Biosensors and Bioelectronics, **19**, pp. 495-502.
5. Gascoyne, P.R.C., Wang, X., Huang, Y., Becker, F.F., 1997, "Dielectrophoretic Separation of cancer cells from blood," IEEE Transactions on Industry Applications, **33**, pp. 670-678.
6. Gascoyne, P.R.C., Satayavivad, J., Ruchirawat, M., 2004, "Microfluidic approaches to malaria detection," Acta Tropica, **89**, pp. 357-369.
7. Lapizco-Encinas, B.H., Simmons, B.A., Cummings, E.B., Fintschenko, Y., 2004, "Insulator-based dielectrophoresis for the selective concentration and separation of live bacteria in water," Electrophoresis, **25**, pp. 1695-1704.
8. Morgan, H., Green, N.G., 1998, "Separation of submicrometre particles using a combination of dielectrophoretic and electrohydrodynamic forces," J. Phys. D: Appl. Phys., **31**, pp. L25-L30.
9. Bennett, D.J., Khusid, B., James, C.D., Galambos, P.C., Okandan, M., Jacqmin, D., Acrivos, A., 2003, "Combined field-induced dielectrophoresis and phase separation for manipulating particles in microfluidics," Applied Physics Letters, **83**, 4866-4868.
10. James, C.D., Khusid, B., Bennett, D.B., Okandan, M., Galambos, P.C., Mani, S.S., Acrivos, A., "Surface micromachined dielectrophoretic gates for the front-end device of a biodetection system," Journal of Fluids Engineering, submitted 2004.
11. Markarian, N., Yeksel, M., Khusid, B., Farmer, K., Acrivos, A., 2003, "Particle motions and segregation in dielectrophoretic micro-fluidics," Journal of Applied Physics, **94**, pp. 4160-4169.
12. Castellanos, A., Ramos, A., Gonzalez, A., Green, N.G., Morgan, H., 2003, "Electrohydrodynamics and dielectrophoresis in microsystems: scaling laws," Journal of Physics D, Applied Physics, **36**, pp. 2584-2597.
13. Okandan, M., Galambos, P.C., Mani, S., Jakubczak, J., 2001, "Development of Surface Micromachining Technologies for Microfluidics and BioMEMS," Proceedings of the SPIE International Society on Optical Engineering, **4560**, pp. 133-139.
14. Laermer, F., Schilp, A., 1996, "Method of anisotropically etching silicon," U.S. Patent Office, Pat No. 5,501,893.
15. Cui, L., Holmes, D., Morgan, H., 2001, "The dielectrophoretic levitation and separation of latex beads in microchips," Electrophoresis, **22**, pp. 3893-3901.
16. Halsey, T.C., "Electrorheological fluids," *Science*, **258**, 761 (1992).

17. Kumar, A., Qiu, Z., Acrivos, A., Khusid, B., and Jacqmin, D., 2004, "Combined negative dielectrophoresis and phase separation in nondilute suspensions subject to a high-gradient ac electric field," Physical Review E, **69**, pp. 021402-1 – 10.

Distribution:

3	MS1080	Conrad James	01769
1	MS1080	Paul Galambos	01769
1	MS1080	David Sandison	01769
1	MS1080	Murat Okandan	01749
1	MS1425	Monica Manginell	01744
1	MS1425	Stephen Casalnuovo	01744
1	MS0892	Susan Brozik	01744
1	MS1413	George Bachand	01116
1	MS9951	Yolanda Fintschenko	08358
1	MS9951	Eric Cummings	08358
1	MS9951	Cindy Harnett	08358
1	MS9403	Timothy Shepodd	08762
1	MS0123	Donna Chavez	01011
1	MS9018	Central Technical File	8945-1
2	MS0899	Technical Library	9616